Sulphur Dioxide Poisoning and Recovery of Platinum Nanoparticles: Effect of Particle Size

M. M. Saleh[1, 2,], M. I. Awad[1,2], F. Kitamura[1], T. Ohsaka[1,*]

[1]Department of Electronic Chemistry, Interdisciplinary Graduate School of Science and Engineering, Tokyo Institute of Technology, 4259 – G1-05 Nagatsuta, Midori-ku, Yokohama 226-8502, Japan
[2] Chemistry Department, Faculty of Science, Cairo University, Egypt
[*]E-mail: ohsaka@echem.titech.ac.jp

The effect of the size of platinum nanoparticles (nano-Pt) deposited onto glassy carbon (GC) electrode (GC/nano-Pt) on the SO_2 poisoning and recovery is examined. Both hydrogen adsorption and oxygen reduction reaction (ORR) are utilized for the quantification of the extent of poisoning and recovery. Cyclic voltammetry (CV) and scanning electron microscopy (SEM) were used to characterize the GC/nano-Pt. Two procedures were used in the recovery of the electrodes activity, i.e., the short-range (1.0 to 0.1 V (vs. RHE)) and long-range (0 to1.5 V) recovery. GC/nano-Pt electrode showed Pt particle size-dependent poisoning-recovery behavior. For the smallest Pt particle size (20 nm) used in the present study the largest extent of the recovery was achieved using either the short-range or long-range recovery procedure. The particles of 20 nm showed ~ 83% current recovery after the short-range recovery and ~100% after the long-range recovery, while those of the largest particle size (480 nm) used in this investigation showed only 67 and 87% current recovery after short-range and long-range recovery, respectively. An attempt to interpret the effects of the nanoparticles size on the poisoning and recovery behavior is introduced. The present experimental framework and analyses may help in the optimization of the Pt particle size in the ORR and the choice of the recovery approach of SO_2 poisoning.

1. INTRODUCTION

Oxygen reduction reaction (ORR) on platinum-based catalysts is one of the most studied electrode reactions due to its equal academic and technological interests. The effects of the size of platinum nanoparticles (nano-Pt) on the ORR have been extensively studied [1-6]. Such effects were studied in alkaline [7,8] and in acid media [9,10]. The size, shape, dispersion and the type of the substrate determine the electroactivity of the nano-Pt towards the ORR [11]. Contradictory effects

have been found among the literatures regarding the influence of the nano-Pt size on the electroactivity of the ORR [12,13]. To the best of our knowledge, there has been no report on the effects of the size of the nano-Pt on the susceptibility to the poisoning by contaminants such as SO_2 and on the recovery of the ORR electroactivity.

Many studies have been found in literature regarding the poisoning of the H_2/Air (O_2) PEM fuel cell by possible contaminants. Most of them have considered the performance of the whole fuel cell under the exposure to different contaminants e.g., SO_2 and H_2S [14-18] and yet only a few studies have examined the behavior of individual electrodes [19-23]. Recently Ramaker et al. [24] studied the poisoning and recovery process for S_x-poisoned nanoscale Pt- and Pt_3Co- on Vulcan carbon (Pt/VC and Pt_3Co/VC) in perchloric acid electrolyte using in situ X-ray absorption spectroscopy. ORR is considerably sluggish compared with the other half reaction in the H_2/Air (O_2) fuel cell, i.e., hydrogen oxidation and hence the study of its poisoning by SO_2 is crucial. Although the H_2/Air (O_2) PEM fuel cell performance depends on the nanosized Pt catalysts, the number of articles regarding the poisoning of nano-Pt modified electrodes is few [25, 26].

The aim of the present article is to investigate the effects of the size of nano-Pt on the poisoning extent and recovery ability of the GC/nano-Pt electrode used for the ORR in acidic media. The present experimental set and analysis may add an insight into the state-of-the-art of nano-scale electrocatalysts that is directed to the H_2/Air (O_2) PEM fuel cell technology. Short-range recovery of the SO_2-poisoned GC/nano-Pt electrode (i.e., cycling the potential between 1.0 and 0.1 V is of interest for the fuel cell recovery at the open circuit potential. On the other hand, long-range recovery (cycling the potential between 0 and 1.5V) is not recommended because of the possible Pt dissolution, but could be essential for the full recovery under specific conditions and restrictions. The range of average sizes of nano-Pt used in this work is 20 to 480 nm which is quite larger than that cited in literature. However, Genies et al. reported threefold decrease in the activity of the ORR when the size of Pt nanoparticles decreases from 24 to 2 nm in alkaline media [7]. Mayrhofer et al. observed similar effects of Pt nanoparticles in perchloric acid media [4]. The durability of extremely small nanoparticles is another criticism for such nanoparticles in application to fuel cells [27]. For the purpose of the present study we can say that the used range (20-480 nm) of the size of the Pt particles is satisfactory.

2. EXPERIMENTAL

Pt nanoparticles-electrodeposited glassy carbon (GC) working electrodes (ϕ = 3 mm in diameter) were used for the cyclic voltammetric (CV) experiments. The counter and reference electrodes were, respectively, a spiral Pt wire and an Ag/AgCl/KCl (sat.). Prior to the electrodeposition of Pt nanoparticles, the GC electrode was polished first with no. 2000 emery paper, then with aqueous slurries of successively finer alumina powder (particle size down to 0.06 μm) with the help of a polishing microcloth. The bare GC electrode was then sonicated for 10 min in Milli-Q water.

All the chemicals were of analytical grade. Pt nanoparticles (nano-Pt) were electrodeposited from 0.1 M H_2SO_4 containing 1 mM H_2PtCl_6 by applying bi-potential steps from the open circuit potential (OCP) to -1.5 V (0.1 s) and then to -0.3 V vs. Ag/AgCl/KCl (sat.) at different time intervals, mainly, 1, 10, 20 and 50 s. The Pt loadings on the GC electrode were estimated from the *i-t* measurements during the electrodeposition as 0.01, 0.018, 0.03 and 0.05 mg cm^{-2} for the time intervals of 1, 10, 20 and 50 s, respectively. The thus-prepared electrodes will be abbreviated as GC/nano-Pt electrodes. The electrodeposition of smaller Pt nanoparticles was carried out from 50 mM H_2SO_4 containing 1 mM H_2PtCl_6 and 20 mM chloride ion. The electrodeposition parameters were the same as above. In this case the loading was 0.011 mg cm^{-2}.

ORR was studied in 0.1 M H_2SO_4 using a conventional two-compartment Pyrex glass container. Milli-Q water (Millipore, Japan) was used to prepare all the solutions. Prior to each experiment, O_2 gas was bubbled directly into the cell for 30 min to obtain an O_2-saturated solution, and during the measurements O_2 gas was flushed over the cell solution. SO_2 poisoning solution was prepared by introducing 0.1M Na_2SO_3 in 0.1M H_2SO_4 solution. In this case Na_2SO_3 (Kanto, Japan) was completely converted to SO_2 soluble in the aqueous solution. That is to say a certain volume of the aforementioned solution was used to prepare the desired concentration of SO_2 in 0.1M H_2SO_4. Then poisoning was done in 5 x 10^{-4} M SO_2 containing N_2-saturated 0.1 M H_2SO_4 by scanning the potential of the electrode (for one cycle) at 0.1 Vs^{-1} between 1.0 and 0.1 V vs. RHE. Next the electrode was transferred into SO_2-free 0.1M H_2SO_4 solution for electrochemical characterization.

Electrochemical measurements were performed at 25 ±1°C using a BAS 100 B/W electrochemical analyzer. The current density was calculated on the basis of the geometric surface area of the underlying GC electrode. Deaeration of the electrolyte solutions was, if necessary, carried out by bubbling N_2 gas for at least 30 min prior to electrochemical measurements. A conventional three-electrode cell of around 20 ml was used for the cyclic voltammetric measurements, while in the case of hydrodynamic voltammetric measurements the working electrode compartment was 200 cm^3 to eliminate any possible changes in the O_2 concentration during the measurements. Steady-state voltammograms were measured at rotating ring-disk electrode (RRDE) with GC-disk ($\phi = 6.0$ mm in diameter) and Pt-ring using a rotary system from Nikko Keisoku, Japan. O_2-saturated solutions were obtained by bubbling O_2 gas for 30 min prior to each experiment and O_2 gas was flushed over the solution during the measurements. The GC disk-Pt ring RRDE was mechanically polished to a mirror surface in the same manner as in the case of the polycrystalline Pt (poly-Pt) electrodes [28] and then was cleaned ultrasonically in Milli-Q water.

3. RESULTS AND DISCUSSION

3.1. Morphological and electrochemical characterization

Figure 1 shows typical SEM images of the GC/nano-Pt electrodes with the average particle sizes of 20, 40 and 90 nm. A considerable uniform size and density distribution of Pt nanoparticles on the surface of the GC electrode can be confirmed from these images. The average sizes of the Pt

nanoparticles were 20, 40, 90, 190 and 480 nm for the electrodes with the loading densities of 0.011, 0.01, 0.018, 0.03 and 0.05 mg cm^{-2}, respectively (see Experimental section). It is noteworthy to mention that the electrodeposition from the $PtCl_6^{2-}$ solution containing chloride ions resulted in a more uniform distribution of nano-Pt with smaller particle size (image A). The smaller particle size could be attributed to the adsorption of chloride ions onto seeded Pt particles and thus prevent the coalescence of the different particles. In addition, the adsorption of chloride ions onto Pt particles brings about a barrier for growth of these particles as it protects them from the further adsorption of $PtCl_6^{2-}$ molecules.
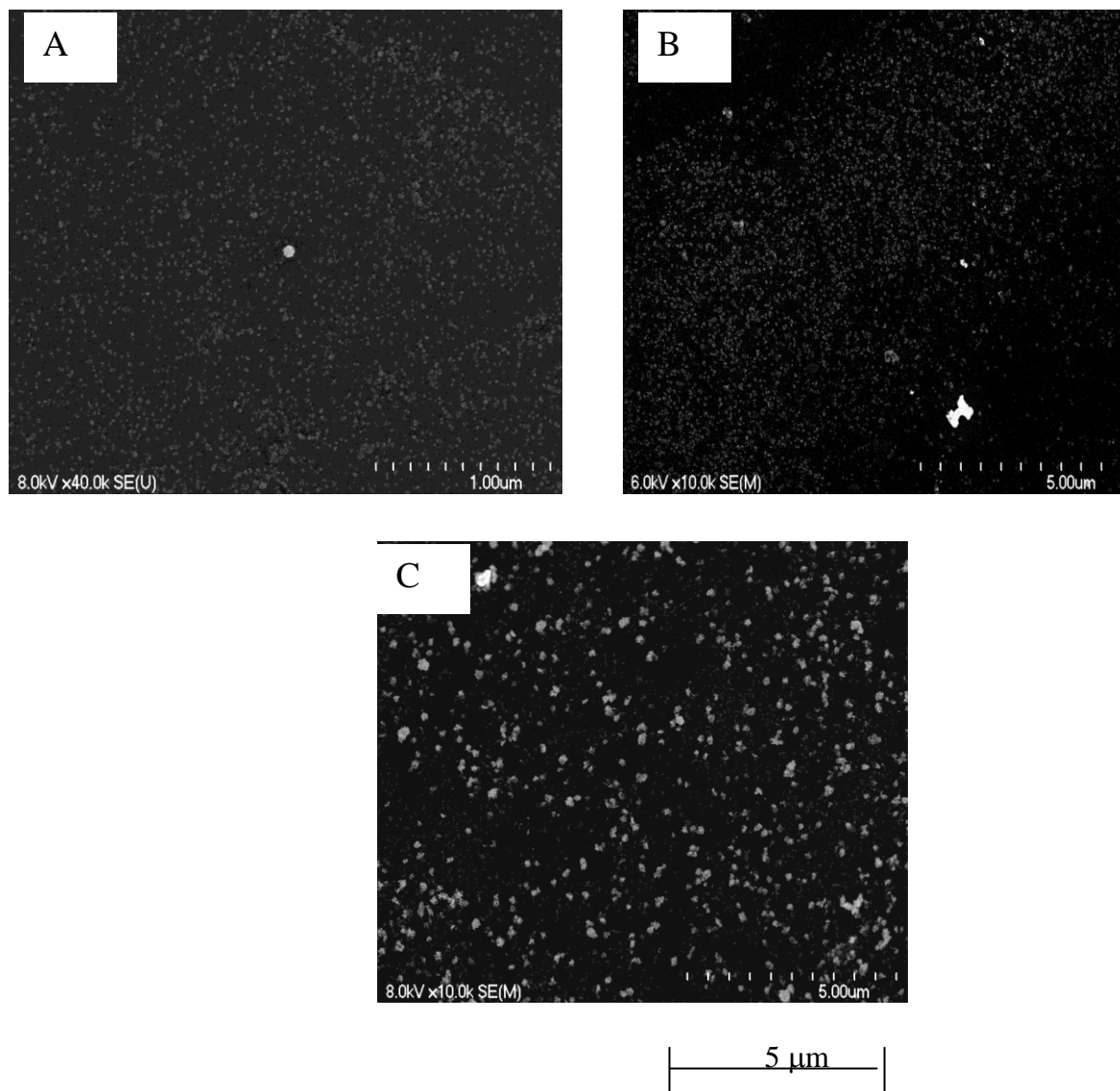
Figure 1. SEM images of GC/nano-Pt electrodes. Average Pt particles sizes: (A) 20, (B) 40 and (C) 90 nm.

Figure 2 shows characteristic CVs of the fresh GC/nano-Pt electrodes of different platinum particle sizes. In general, the cathodic peak potential corresponding to the reduction of the platinum

oxide (Pt-O) obtained at 0.6-0.7 V shifts to the more positive value with an increase in the particle size from 20 to 480 nm. The CV obtained at the nano-Pt of 20 nm size is not presented for the sake of simplicity. Such a positive potential shift with increasing the particle size has been reported to be attributed to a stronger binding of the adsorbed oxygen to the Pt of smaller particle size due to the low-coordination Pt sites (Pt with low coordination number) such as corners, edges and defects [29]. The electrochemical surface area (ECSA) was estimated from the H(adsorption/desorption) ($H_{ads}/_{des}$) peaks in Fig. 2 where 1 cm^2 is equivalent to 210 μC [30]: 0.070, 0.028, 0.035, 0.059 and 0.097 cm^2 for the average particle sizes of 20, 40, 90, 190 and 480 nm, respectively. Note that the electrode with the average size of 20 nm has a larger particle density (loading) (image A in Fig.1), and thus ECSA is larger compared to the electrodes of particle sizes of 40, 90 and 190 nm.
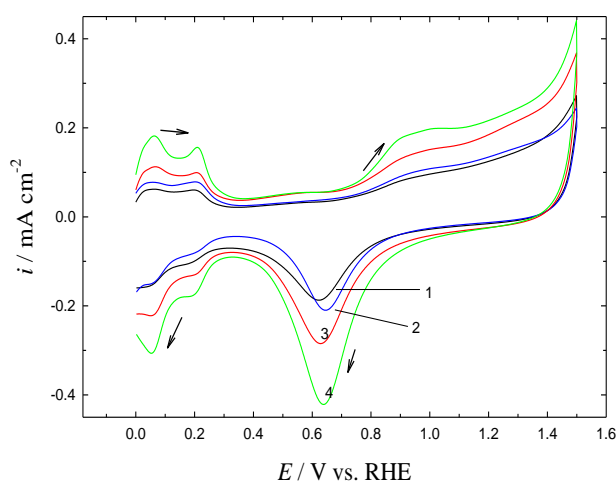
Figure 2. CVs obtained at the GC/nano-Pt electrodes with different sizes of the Pt particles in N_2-saturated 0.1 M H_2SO_4. Average particle sizes: (1) 40, (2) 90, (3) 190 and (4) 480 nm. Potential scan rate : 0.1 V s^{-1}.

It is noteworthy to mention that the poisoning effect of bisulfate, that may interfere with the poisoning of sulfur dioxide, is severe at Pt(111) single crystalline electrode compared with its effect at the other two low facets, i.e., Pt(110) and Pt(100) [31]. At polycrystalline Pt electrode (as in the present case) it has been reported that the adsorption of SO_4^{2-} has little effects on the kinetics of the ORR in acidic sulfate media [31]. In addition it has been reported that the poisoning effect of bisulfate in PEM fuel cells is minimized by humidity [32]. Thus in solutions, in the present case, it could be expected that the effect of bisulfate adsorption is negligible.

3.2. Poisoning of the GC/nano-Pt electrodes

Figure 3 shows the CV behavior of GC/nano-Pt electrodes of different Pt particle sizes in N_2-saturated 0.1 M H_2SO_4 solution containing 5×10^{-4} M SO_2. The potential was scanned initially in the negative direction of potential. Starting from the potential of 0.6 V, a cathodic region with the

reduction of SO_2 to SO_x and sulphur was obtained. At potential more negative than 0.3 V elemental sulphur is a possible product of the reduction of SO_2 [33, 34]. At the potential range 0.65-0.75 V an anodic peak (indicated by an arrow) was observed which is assigned for the oxidation of soluble SO_2. Such a peak appears only when the potential (scanned initially in the negative direction of potential) was reversed at a certain value sufficient for the formation of adsorbed sulfur of certain coverage [34].
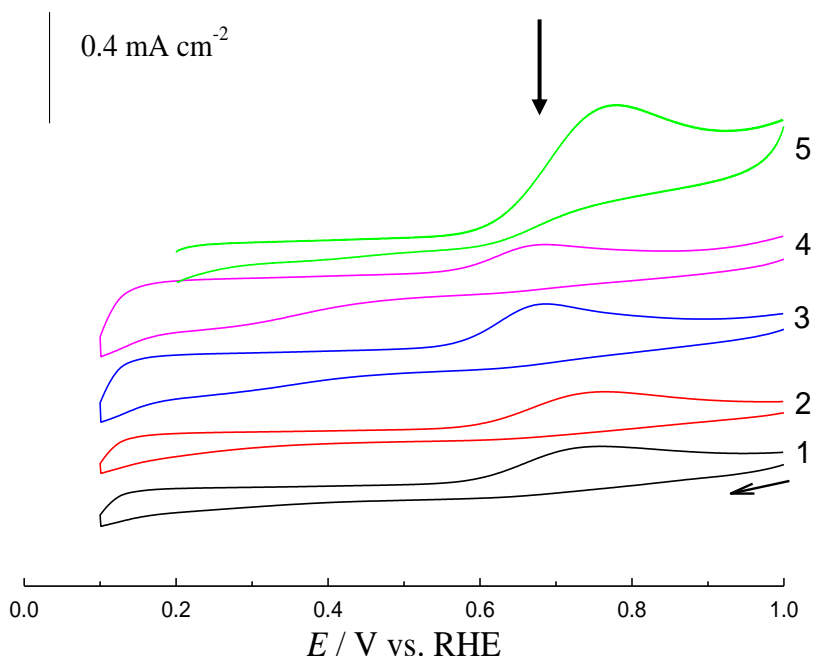
Figure 3. CVs obtained at GC/nano-Pt electrodes in N_2-saturated 0.1 M H_2SO_4 containing 5×10^{-4} M SO_2. Average particle sizes: (1) 40, (2) 90, (3) 190 and (4) 480 nm. Curve 5 is the results obtained at poly-Pt electrode. Potential scan rate : 0.1 V s^{-1}.

This peak was confirmed with polycrystalline Pt electrode (1.6 mm diameter) treated similarly as shown in curve 5 of Fig. 3. The appearance of this peak is an evidence of the formation of elemental sulphur layer on the electrode surface since elemental sulphur species has been reported to enhance the oxidation of SO_2 in solution [35-37]. The change of the anodic peak potential with the particle size is not significant since it has been reported that a certain optimum loading of sulfur may activate the SO_2 oxidation [35-37]. After the above poisoning process the fraction of the platinum surface covered by sulphur (surface coverage) was estimated from the amount of charge consumed in the hydrogen desorption obtained in N_2-saturated 0.1 M H_2SO_4, typically in Fig. 9 for the particle of 40 nm size. The sulphur surface coverages were found to be 0.90, 0.79, 0.88, 0.77 and 0.79 for the particles of the average sizes of 20, 40, 90, 190 and 480 nm, respectively.

For estimating the number of S atoms adsorbed on the different electrodes, the potential scan was repeated several times in N_2-satuaretd 0.1 M H_2SO_4 in the range of -0.4 to 1.5 V until the characteristic CV of a clean Pt electrode was obtained. The CVs shown in Fig. 4 are for the GC/nano-

Pt electrode with the average particle size of 190 nm. Similar CVs were also obtained for the electrodes of the other particle sizes. Upon cycling the potential, the anodic peak at ca. 1.2 V decreases and the onset potential of the Pt oxidation shifts cathodically. In addition, the decrease in the anodic peak at 1.2 V with cycling is accompanied by a continuous increase in the reduction peak at ca. 0.65 V. This indicates the regeneration of the clean Pt surface via the oxidative removal of sulphur. Note that the last CV (see arrows in the figure) is identical with that obtained for the fresh electrode as shown in Fig. 2. Then the amount of adsorbed S was estimated by subtracting the charge corresponding to the reduction of the platinum oxide layer concurrently formed during the anodic scan from the anodic charge corresponding to both the oxidative removal of S and the platinum oxide layer formation. This subtraction was repeated over the number of potential cycles necessary for obtaining the response of the fresh electrode and the total amount of the adsorbed S was estimated from the following Eqn.; [25]

$$Q_s = \sum_n (Q_n^a - Q_n^c) \tag{1}$$

where Q_n^a and Q_n^c are the anodic and cathodic charge, respectively, at the nth cycle.
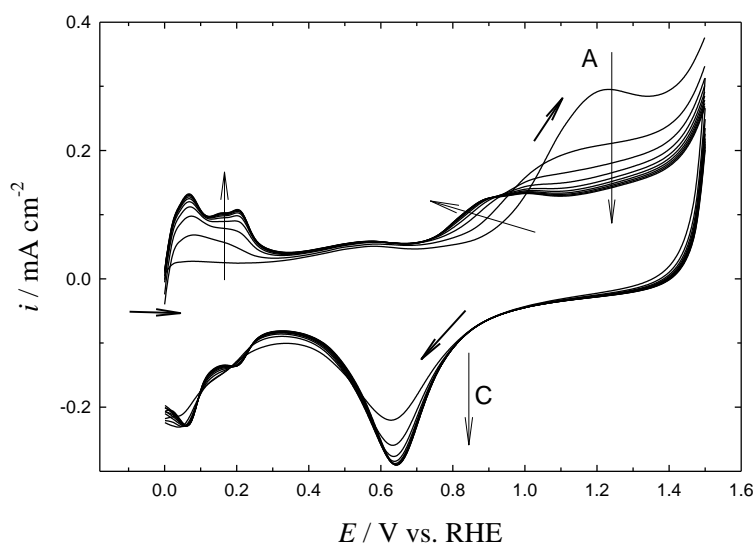
Figure 4. Sequence of CVs obtained at the poisoned GC/nano-Pt electrode with average particle size of 190 nm in N_2-saturated 0.1 M H_2SO_4. Potential scan rate : 0.1 V s^{-1}.

Using the values of Q_s in Eqn.1 and assuming 6e for the electrochemical oxidation of S to sulphate ion (see Eqn. 2), the number density of sulphur sites was estimated to be 1.2×10^{15}, 2.0×10^{15}, 1.8×10^{15}, 1.2×10^{15} and 9.4×10^{14} S sites/cm^2 (ECSA) for the particles of average sizes of 20, 40, 90, 190 and 480 nm, respectively. The number of atoms per unit area has been reported to be around 10^{15} atoms/cm^2. The comparable calculated values indicate that a sulfur monolayer is formed at all the studied electrodes. Also a little variation in the number density of sulfur might be due to the difference in coordination of S to the nano-Pt, i.e., it might be a single or multi coordination [14, 21,

38] and/or the difference in the crystallographic orientation of the different nanoparticles modified electrodes.

3.3. Recovery of the poisoned electrodes

In order to study the recovery extent of the ORR activity at the different particle sizes, a fresh GC/nano-Pt electrode was poisoned as done in Fig. 3 and then it was transferred to SO_2-free 0.1 M H_2SO_4 solution and the ORR was measured (see Fig.5). Figures 5 A and B show the ORR on the GC/nano-Pt electrode with the Pt particle sizes of 40 and 90 nm, respectively. Those are the CVs for the ORR on the fresh electrode (curves 1), on the poisoned electrode (curves 2), after the 5th and the 10th potential cycle of the short-range recovery (curves 3 and curves 4, respectively) and after the long-range recovery (curves 5). The long-range recovery was achieved by cycling the potential three times between 0 and 1.5 V in N_2-satuaretd 0.1 M H_2SO_4. In the procedure of the short-range recovery(SRR) the potential was cycled sequentially for 10 cycles in the range of 1.0 to 0.1 V in O_2-saturated 0.1 M H_2SO_4 solution (SO_2-free). As a result, the peak current is improved and the peak potential of ORR shifts to the positive direction of potential (compared to the poisoned electrode). The gradual improvement of the potential and the current with cycling is due to the desorption of weakly bound sulphur from the GC/nano-Pt surface [24,26]. By the 10th cycle a remarkable improvement was observed, but fully recovered activity of the ORR was not obtained. Competitive adsorption of the O_2 molecule could assist such desorption of the weakly bound sulphur. Also we may consider the partial electrochemical oxidation of sulphur (PEOS) at the positive end, i.e., 1.0 V, in the SRR protocol, (see Fig.5) and a possible chemical reaction between surface sulphur and the H_2O_2 generated during the ORR [14]. The PEOS as a possible reason for recovery of the poisoned electrode was confirmed by decreasing the potential range for recovery to be between 0.8 and 0.1 V and it was found that the recovery is negligible (data are not shown). This indicates that the PEOS does play a role in the recovery of the electrode using the SRR protocol. Similar CV results were obtained for the electrodes of the other particle sizes (20, 90, 190 and 480 nm) and the results are summarized in Figs. 6 and 7.

Figure 5 clearly shows the improvement in the ORR activity upon the short-range recovery especially after the 10th cycle with a greater ORR improvement of the Pt particles of 40 nm than that of 90 nm. However, the full recovery (for the 40 nm) and nearly full recovery (for the 90 nm) were obtained only after the long-range recovery treatment. This can be attributed to the oxidation of the strongly bound sulphur species (at potential > 1.2V) on the GC/nano-Pt surface to soluble sulphate ions according to the following equation;

$$S \;\; + \;\; 4H_2O \;\;\; = \;\;\; SO_4^{2-} \;\; + \;\; 8H^+ + \;\; 6e^- \tag{2}$$

Similar CVs were also obtained for the particles of the other sizes (*i.e.*, 20, 190 and 480 nm) (data are not shown).
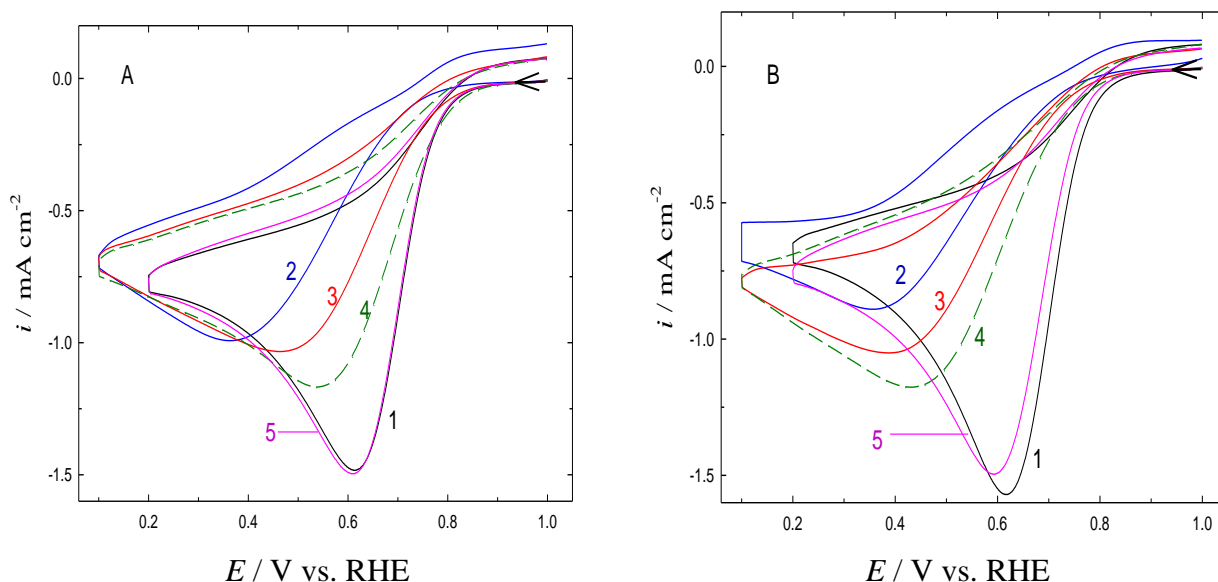
Figure 5. ORR in SO$_2$-free 0.1 M H$_2$SO$_4$ on the GC/nano-Pt electrode. (1) fresh electrode, (2) poisoned (3) and (4) after the 5th and the 10th cycles of the short-range recovery, respectively and (5) after the long- range recovery. Average Pt particles size: (A) 40 and (B) 90 nm.

The percentage recovery of the peak current of the ORR, *Rec* (%) after the above treatment (the short- and long-range recovery) can be given by;

$$Rec = \frac{i_{rec}}{i_{bare}} \times 100 \qquad\qquad (3)$$

where i_{rec} and i_{bare} are the peak currents of the ORR on the recovered and bare (fresh) electrodes, respectively. The *Rec* values after every potential cycle (up to 12 potential cycles) in the treatment by short-range recovery were calculated at the electrodes of different particle sizes and are shown in Fig. 6. It can be seen that the current recovery gradually increases with increasing the number of potential cycle and attains an almost constant value at the 10th cycle. At the poly-Pt electrode the current recovery does not significantly increase with increasing the number of potential cycles. At the same cycle number, the smaller the particle size, the larger the *Rec* (see Fig. 7). The dependence of the *Rec* on the particle size is summarized in Fig. 7 under the different ways of recovery of the GC/nano-Pt electrodes of different Pt particle sizes. Curve a shows the percentage current recovery after the 10th cycle in the short-range recovery, while curve b in the long range recovery. It is noteworthy to mention that although the number density of S on the GC/nano-Pt electrode of the particle size of 20 nm is comparable with that at other modified electrodes, it shows the best recovery by the above-mentioned short-range recovery procedure.
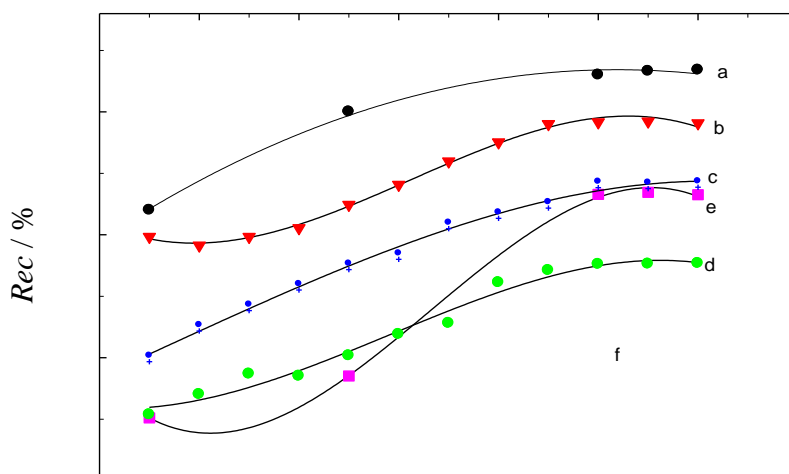
Figure 6. Percentage current recovery change of the ORR peak current with the number of potential cycles in the short-range recovery (1.0 to 0.1 V) obtained at GC/nano-Pt electrodes with different platinum nanoparticles sizes: (a) 20, (b) 40, (c) 90 and (d) 480 nm. (e) was obtained at poly-Pt electrode.

We can say that the enhanced recovery at the smaller particle size is not due to the difference in the loading at the different electrodes, because when the nano-Pt of 20 nm was deposited with a comparable loading to the nano-Pt of 40 nm, the maximum recovery was obtained at the former electrode. With the long-range recovery, a 100% recovery was obtained at the GC/nano-Pt electrodes of Pt particle sizes 20 and 40 nm, but the lower *Rec* values were obtained for the other particles of larger sizes. The highest recovery was obtained at the nano-Pt of the particle size of 20 nm.

In Fig. 5 the peak current of the 1st cycle obtained at the poisoned electrode (curves 2) is almost half of that obtained at the fresh electrode (curves 1). Similar results were obtained at the other GC/nano-Pt electrodes. To clarify the reason behind this significant decrease in the current, i.e., whether it is due to the decrease in the active surface area or the change in the mechanism of the ORR, the rotating ring-disk electrode (RRDE) voltammetry at the different electrodes was conducted. The results obtained at the GC/nano-Pt (190 nm) electrode are shown typically in Fig 8 in which disk currents (a-d) were obtained at (a) fresh and (b) poisoned electrodes, (c) recovered electrode (by 10 potential cycles in the short-range) and (d) recovered electrode (by 3 potential cycles in the long-range) and the corresponding ring currents (a'-d') for the H_2O_2 oxidation at the Pt-ring electrode at a rotation rate of 800 rpm. The Pt-ring electrode was potentiostated at 1.2 V at which the oxidation of H_2O_2 is diffusion-controlled. In curve a the ring current is significantly small indicating the exclusive 4-electron reduction of O_2 to H_2O.

Particle size / nm
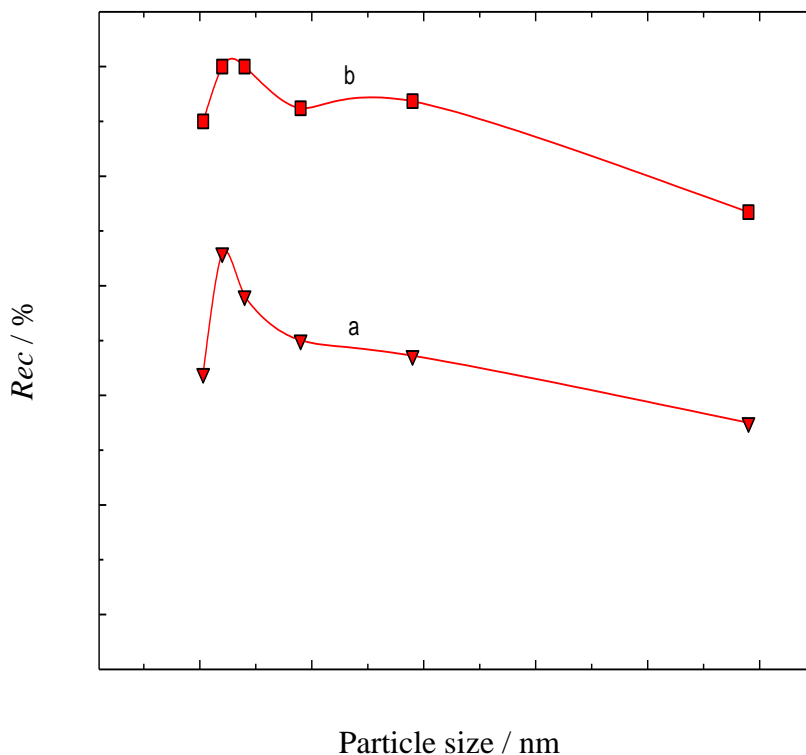
Figure 7. Percentage current recovery of the ORR peak current (a) after the 10th cycle of the short-range recovery and (b) after the long-range recovery.

Whereas, in the case of the poisoned electrode (curve b) the disk current is almost half that obtained at the fresh electrode and the ring current is significantly large indicating the significant contribution of the 2-electron reduction (formation of H_2O_2) due to the adsorption of sulfur species which might partially change the adsorption pattern of molecular oxygen form a parallel mode to an end top mode. Such a change in the ORR mechanism occurs because of the decrease in the number of adjacent adsorption sites necessary for a parallel-mode adsorption of oxygen molecule resulting in the breaking of the O-O bond [39]. The percentage of the electrogenerated hydrogen peroxide ($X_{H_2O_2}$) at potential 0.2 V, as estimated by Eq. 4 where I_R and I_D are the ring and disk currents, respectively and N is the collection efficiency (equal 0.42), was found to be 10 and 78 % at the fresh and poisoned electrodes, respectively.

$$X_{H_2O_2} = \frac{\dfrac{2I_R}{N}}{I_D + \dfrac{I_R}{N}} \tag{4}$$
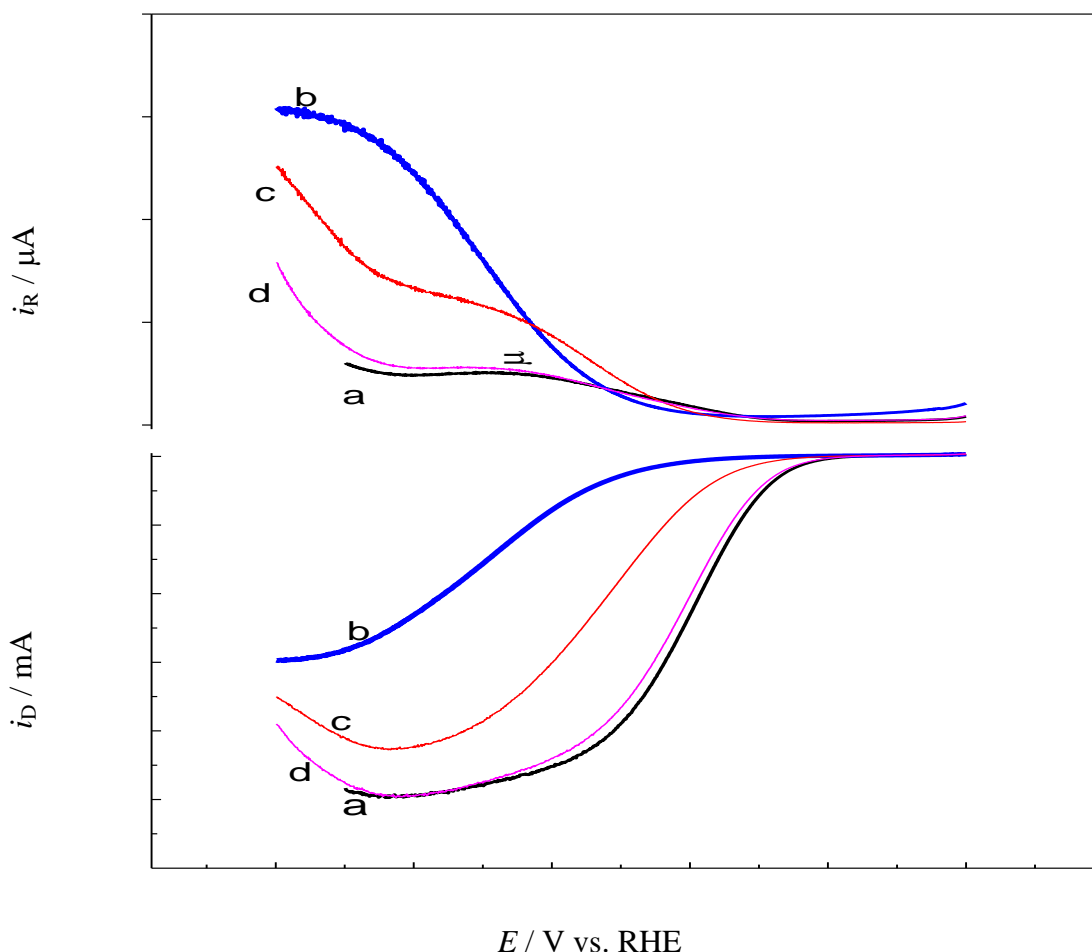
Figure 8. Steady-state voltammograms for the ORR obtained at (a-d) GC/nano-Pt electrode (average Pt particle size:190 nm) ((a)fresh, (b) poisoned, (c) recovered by 10 potential cycles in the short-range potential and (d) recovered by 3 potential cycles in the long-range potential) and (a′, b′, c′, d′) Pt ring electrode in O_2-saturated 0.1 M H_2SO_4 solution. Rotation rate: 800 rpm and the Pt ring was potentiostated at 1.2 V vs. RHE. Potential scan rate: 10 mVs^{-1}.

Curve c obtained after the short-range recovery is improved; however still the relevant ring current is large pointing out that the short-range recovery is not sufficiently remedial in the present case. In curve d, which is obtained after the long-range recovery, the RRDE voltammetric behavior is almost similar to that at the fresh electrode. This means that the electrode is completely recovered under these conditions of recovery.

The recovery of the peak potential of the ORR on the GC/nano-Pt electrodes with different particle sizes is shown in Table 1. It shows the differences between the peak potentials of the ORR obtained at the individual fresh electrodes and after the short- and long-range recovery of the poisoned electrodes. Using the long-range recovery procedure all the electrodes were almost completely recovered in terms of the ORR peak potential.

Table 1. The differences between the peak potentials of the ORR obtained at the fresh electrodes (E_{fresh}) and the recovered electrodes after short-range (E_{5th} and E_{10th}) and long-range (E_{LRR}) recovery for the different electrodes.

Average Particle Size, nm	$(E_{\text{fresh}} - E_{\text{5th}})^{\text{a}}$/V	$(E_{\text{fresh}} - E_{\text{10th}})^{\text{a}}$/ V	$(E_{\text{fresh}} - E_{\text{LRR}})^{\text{b}}$/V
20	0.134	0.06	0.00
40	0.131	0.056	0.00
90	0.160	0.070	0.030
190	0.146	0.099	0.021
480	0.106	0.047	0.004
Poly-Pt	0.350	0.170	0.110

[a] E_{5th} and E_{10th} are the peak potentials of the ORR obtained at the electrodes recovered by five and ten potential cycles , respectively, in the potential range of 1.0 ~ 0.1 V.
[b] E_{LRR} is the peak potential of the ORR obtained at the electrodes recovered by three potential cycles in the potential range of 0 ~ 1.5 V.

The estimation of the electrochemical surface area (ECSA) of the GC/nano-Pt electrodes from the characteristic CVs of the hydrogen adsorption-desorption ($H_{\text{ads}}/_{\text{des}}$) could be used as quantification for the effect of the recovery procedures, i.e., the short- and long-range recovery. This is shown in Fig. 9 typically for the 40 nm particle size. The *A* values for the bare, poisoned and recovered electrodes were estimated from the values (Q) of charge consumed in the hydrogen desorption. Then the surface coverage (θ) of sulphur was calculated from the following relation;

$$\theta = 1 - \frac{Q}{Q^o} \qquad\qquad (5)$$

where Q^o and Q are the amounts of charge consumed in the hydrogen desorption at the fresh (bare) and poisoned (or recovered) GC/nano-Pt electrodes, respectively. The thus-obtained values of Q, A and θ of the different electrodes (i.e., fresh, poisoned and recovered) are given in Table 2. From this Table we can see that the θ values of the GC/nano-Pt electrodes are a good reflection for the current recovery estimated from Fig. 5A. For instance, the *Rec* values for the GC/nano-Pt (40 nm) are 79 and ~100% after the short-range (after the 10th cycle) and long-range recovery, respectively, while the corresponding θ values are 0.16 and 0.002. One can easily see that the extent of poisoning, i.e., the sulfur surface coverage (equals 0.83 ± 0.07) of poisoned electrodeposited nano-Pt modified electrodes, does not change significantly with the size of platinum nanoparticles. On the other hand the surface coverage of the electrodes recovered by short-range and long-range recovery procedures increases systematically with increasing the particles size. This indicates that the size of the platinum nanoparticles plays a crucial role in the recovery ability of these electrodes.
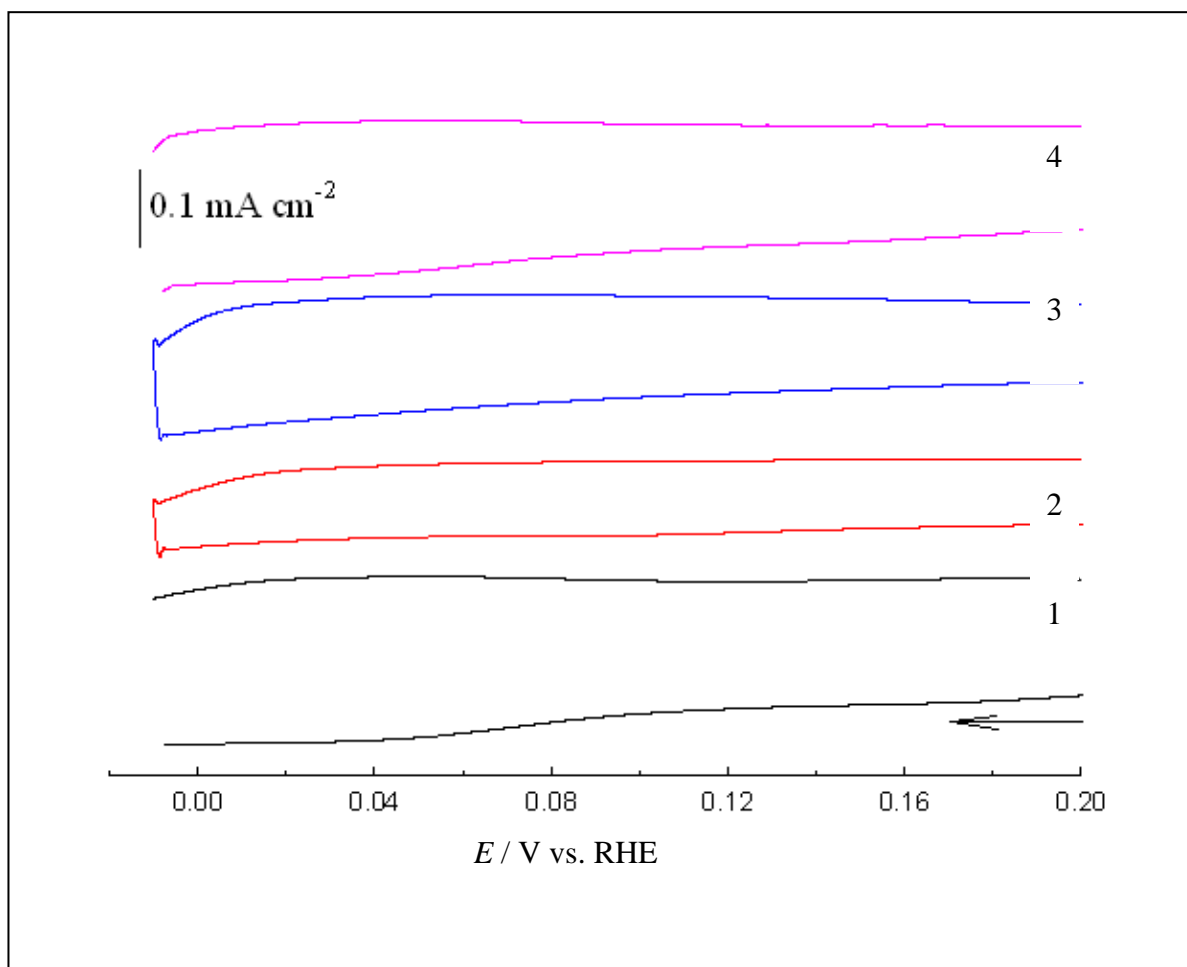
Figure 9. CVs of the $H_{ads/des}$ on the GC/nano-Pt (average Pt particle size: 40 nm) in N_2-staurated 0.1 M H_2SO_4: (1) fresh electrode, (2) poisoned electrode, (3) after short-range recovery and (4) after long-range recovery.

In order to confirm the above correlations, the data on polycrystalline Pt (Poly-Pt) electrode is also taken into account. CVs for the ORR similar to those shown in Fig. 4 were obtained for the Poly-Pt electrode (data are not shown here) and the surface coverages were estimated (Table 2). It was found that the *Rec* values at the Poly-Pt after the short-range (10th cycle) and the long-range recovery were 60 and 75%, respectively. Also the negative shift in the peak potential after the long-range recovery was 110 mV. Thus, the results obtained at the Poly-Pt confirm the above-mentioned correlations and the lower *Rec* values were obtained on the Poly-Pt with respect to the GC/nano-Pt of the largest particle size (480 nm).

An attempt to explain and rationalize the above-mentioned results can be introduced in the following. Possible formation of Pt-O can activate the oxidation of sulphur to soluble sulphate ions in the potential range between 1.0 and 1.5 V [39, 40]. Figure 10 shows the CVs obtained at the first potential cycle in the long-range recovery (see Fig. 4) of the poisoned GC/nano-Pt electrodes with particle sizes of 40 nm (curve A) and 90 nm (curve B) and of the poisoned Ploy-Pt electrode (curve C). We can see that both the onset potential of the S oxidation and the Pt-O reduction potential peak are

more positive in the following order: GC/nano-Pt (40 nm) electrode < GC/nano-Pt (90 nm) electrode < Poly-Pt electrode. It means that the S oxidation occurs more easily at the smaller Pt particle. Yet we can say that the strongly bound Pt-O enhances the S oxidation reaction on the electrode surface as reported previously [40, 41]. This may explain the favorable S oxidation on the GC/nano-Pt (40 nm) over the other Pt particle sizes and also confirms the higher percentage of current recovery obtained on the smaller Pt particle size shown in Fig. 7.

Table 2. Electrochemical surface area (ECSA), charge consumed in the hydrogen desorption (Q) and surface coverage of sulphur (θ).

Electrodes	Charge (Q)/μC				ECSA /cm$^{2\ a}$				Surface coverage (θ)		
	bare	Poisoned [b]	SRR [c]	LRR [d]	bare	Poisoned [b]	SRR [c]	LRR [d]	Poisoned [b]	SRR [c]	LRR [d]
GC/nano-Pt (20 nm)	14.7	1.47	13.1	14.68	0.07	0.007	0.062	0.069	0.90	0.11	0.001
GC/nano-Pt (40 nm)	5.8	1.26	4.45	5.81	0.028	0.006	0.023	0.028	0.79	0.16	0.002
GC/nano-Pt (90 nm)	7.4	0.89	5.03	6.07	0.035	0.004	0.024	0.029	0.88	0.32	0.18
GC/nano-Pt (190 nm)	10.1	2.30	5.95	7.10	0.059	0.010	0.028	0.033	0.77	0.41	0.29
GC/nano-Pt (480 nm)	19.4	2.40	5.8	13.1	0.097	0.011	0.027	0.067	0.79	0.70	0.32
poly-Pt	12.0	0.63	1.89	9.24	0.057	0.003	0.009	0.044	0.95	0.84	0.24

[a] As estimated from the amount of charge consumed in the hydrogen desorption using 210 μC/cm^2 [26].
[b] The GC/nano-Pt electrode was poisoned by cycling the potential between 1.0 and 0.1 V in deaerated 0.1 M H_2SO_4 containing 5.0 x 10^{-4} M SO_2.
[c] As recovered by the short-range recovery, i.e., by cycling the potential between 1.0 and 0.1 V in O_2-saturated 0.1 M H_2SO_4.
[d] As recovered by the long-range recovery, i.e., by cycling the potential between 0.0 and 1.5 V in O_2-saturated 0.1 M H_2SO_4.

Another probable explanation is the possibility of stronger adsorption of sulfate ion on the smaller size of Pt-nanoparticles due to low-coordination Pt sites such as corners, edges and defects [29]. Sulfate ions can adsorb on the platinum electrode surface in the potential range of 1.0-0.6 V with an adsorption extent depending on the sulfate ion concentration [42]. Note that the sulfate ion concentration (0.1 M H_2SO_4) in this study is 2x10^4 times greater than the SO_2 concentration. Although the stronger adsorption of SO_4^{2-} can have little effects on the kinetics of the ORR in acidic sulfate medium [42], it can have a stronger effect on the adsorbability of SO_2 on the Pt-nanoparticles. That is to say, the competitive adsorption of SO_4^{2-} and SO_2 on the smaller nanoparticles may help in retarding the adsorption of SO_2 but it does not affect the kinetics of the ORR. We can say that the adsorption of SO_4^{2-} can not prevent the adsorption of O-O to Pt-surface, but it can compete with the SO_2 adsorption.
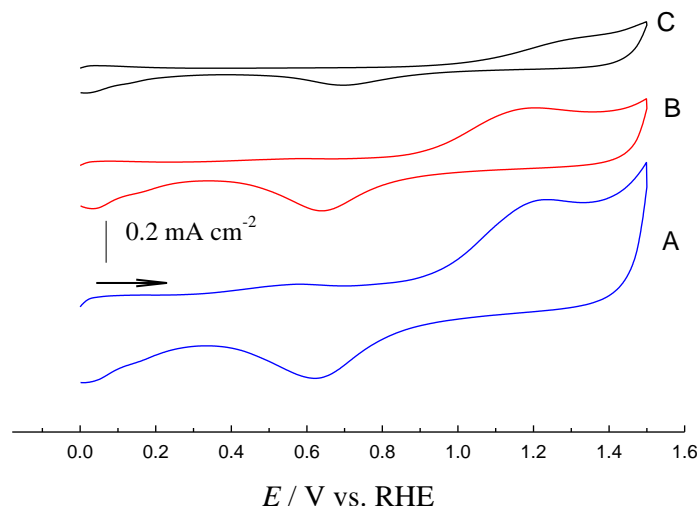
Figure 10. CVs obtained at the poisoned GC/nano-Pt electrodes with average Pt particle sizes of (A) 40 and (B) 90 nm and (C) at the poly-Pt electrode in N_2-saturated 0.1 M H_2SO_4. Potential scan rate: 0.1 Vs^{-1}.

4. SUMMARY and CONCLUSIONS

This study was dedicated to examine the effects of the Pt particle size on the SO_2 poisoning and recovery of GC/nano-Pt electrode in the ORR in H_2SO_4 solution. The smaller particle showed the easier recovery upon applying either short-range or long-range recovery. RRDE experiments show that sulphur is detrimental to the ORR reaction because it promotes a 2-electron pathway to yield H_2O_2. The higher percentage of current recovery at the smaller particle was attributed to either a stronger binding of the Pt-O or to a higher adsorbability of the sulfate ion which competes with the adsorption of SO_2 due to the low-coordination Pt sites.

References

1. O. Antoine, Y. Bultel, R. Durand, and P. Ozil, *Electrochim. Acta*, 43 (1998) 3681.
2. K. Kinoshita, *J. Electrochem. Soc.*, 137 (1990) 845.
3. H. Ye, J. A. Crooks, R. M. Crooks, *Langmuir* 23 (2007) 11901.
4. K. J. Mayrhofer, B. B. Blizanac, M. Arenz, V. R. Stamenkovic, P. N. Ross, and N. M. Markovic, *J. Phys. Chem.* B, 109 (2005)14433.

5. Y. Takasu, N. Ohashi, X. G. Zhang, Y. Murakami, H. Minagawa, S. Sato, and K. A.Yahikozawa, *Electrochim. Acta*, 41 (1996) 2595.
6. H. A Gasteiger, S. S. Kocha, B. Sompalli, F. T. Wagner, *Appl. Catal. B: Environ.* 56 (2005) 9.
7. L. Genies, R. Faure, and R. Durand, *Electrochim. Acta,* 44 (1998) 1317.
8. J. Perez, E. R. Gonzalez, E. A. Ticianelli, *Electrochim. Acta*, 44 (1998) 1329.
9. H. Yano, J. Inukai, H. Uchida, M. Watanabe, P. K. Babu, T. Kobayashi, J. Ho Chung, E. Oldfield, A. Wieckowski, *Phys. Chem. Chem. Phys*., 8 (2006) 4932.
10. C. Wang, H. Daimon, T. Onodera, T. Koda, S. Sun Angew. *Chem. Int. Ed*., 47 (2008) 3588.
11. J. Wang, G. Yin, Y. Shao, Z. Wang, Y. Gao, *J. Electrochem. Soc*., 154 (2007) B687.
12. S. H. Jooa, K. Kwon, D. J. Youa, C. Pak, H. Chang, J. Kim, *Electrochim. Acta*, 54 (2009) 5746.
13. M.Watanabe, H. Sei, P. Stonehart, *J. Electroanal. Chem*., 261 (1989) 375.
14. Jie Fu, M. Hou, C. Du, Z. Shao, B. Yi, *J. Power Sources* 187 (2009) 32.
15. R. Halseid, M. Heinen, Z. Jusys, R. Behm, *J. Power Sources*,176 (2008) 435.
16. R. Mohtadi, W.-k. Lee, S. Cowan, J. W. Van Zee, and M. Murthy, *Electrochem. Solid-State Lett*., 6 (2003) A272.
17. D. T. Chin and P. D. Howard, *J. Electrochem. Soc.,* 133 (1986) 2447.
18. X. Cheng, Z. Shi, N. Glass, Lu Zhang, J. Zhang, D. Song, Z. Liu, H. Wang, J. Shen, *J. Power Sources,* 165 (2007) 739.
19. C. Quijada, J. L. Vazquez, A. Aldaz, *J. Electroanal. Chem*. 414 (1996) 229.
20. T. Loucka, *J. Electroanal. Chem*. 31 (1971) 319.
21. M. I. Awad, M. M. Saleh, T. Ohsaka, *J. Power Sources* 196 (2011) 3722.
22. M. Abdullah, M. M. Saleh, M. I. Awad, T. Okajima, F. Kitamura, T. Ohsaka, *J. Solid State Electrochem.*, 14 (2010)1727.
23. C. Quijada, J. L. Vázquez, *Electrochim. Acta* 50 (2005) 5449.
24. D. E. Ramaker, D. Gatewood, A. Korovina, Y. Garsany, and K.E. Swider-Lyons, *J. Phys. Chem. C*, 114 (2010) 1886.
25. Y. Garsany, O. A. Baturina and K. E. Swider-Lyons, *J. Electrochem. Soc.* 154 (2007) B670.
26. Y. Garsany, O. A. Baturina, K. E. Swider-Lyons, *J. Electrochem. Soc.*, 156 (2009) B848.
27. Y. Tsou, L. Cao, E. De Castro, *ECS Transactions*, 13 (2008) 67.
28. J. Maruyama, M. Inaba, Z. Ogumi, *J. Electroanal. Chem.*, 458 (1998) 175.
29. B. E. Hayden, D. Pletcher, J. Suchsland, L. J. Williams, *Phys. Chem. Chem. Phys*., 11 (2009) 9141.
30. S. Trasatti, O. A. Petrii, *Pure and Appl. Chem*., 93 (1991) 711.
31. M. D. Macia, J. M. Campina, E. Herrero, J. M. Feliu, *J. Electroanal. Chem*. 564 (2004) 141.
32. Y. Nagahara, S. Sugawara, K. Shinohara, *J. Power Sources* 182 (2008) 422.
33. C. Quijada, A. Rodes, J.L. Vazquez, J.M. Perez, A.Aldaz, *J. Electroanal. Chem*. 394 (1995) 217.
34. C. Quijada, A. Rodes, F. Huerta, J. L. Vazquez, *Electrochim. Acta* 44 (1998) 1091.
35. S. Lee, C. Kim, W. Cho, K. Kang, C. Park, K. Bae, *Int. J. Hydrogen Energy*, 34 (2009) 4701.
36. R. M. Spotnitz, J. A. Colucci, S. H. Langer, *Electrochim. Acta*, 28 (1983) 1053.
37. C. Quijada, A. Rodes, J. L. Vázquez, J. M. Pérez, A. Aldaz, *J. Electroanal. Chem.* (1995) 105.
38. A. Q. Contractor, H. Lal, *J. Electroanal. Chem*., 96 (1979) 175.
39. S. Imabayashi, Y. Kondo, R. Komori, A. Kawano, T. Ohsaka, *ECS Trans*. 16 (2008) 925.
40. K. E. Swider, D. R. Rolison, *Langmuir*, 15 (1999) 3302.
41. K. E. Swider, D. R. Rolison, *J. Electrochem. Soc*., 143 (1996)813.
42. M.D. Macia, J. M. Campina, E. Herrero, J.M. Feliu, *J. Electroanal. Chem.,* 564 (2004) 141.